frontiers in Earth Science

ORIGINAL RESEARCH
published: 29 January 2021
doi: 10.3389/feart.2020.574385

The Van Microplate: A New Microcontinent at the Junction of Iran, Turkey, and Armenia

Hossein Azizi[1]* *and Motohiro Tsuboi*[2]

[1]Department of Mining, Faculty of Engineering, University of Kurdistan, Sanandaj, Iran, [2]Department of Applied Chemistry for Environment, School of Science and Technology, Kwansei Gakuin University, Sanda, Japan

In northwestern Iran, magmatic activity occurred during three main intervals: The Cretaceous, Eocene, and Miocene-Quaternary. The first two phases of magmatic activity are more consistent with arc-type magmatism on an active continental margin; whereas the last phase, which has calc-alkaline and alkaline affinities, shows more similarity to postcollisional magmatism. Magmatic belts are mostly situated in the northern and eastern parts of the Oshnavieh–Salmas–Khoy ophiolite belt (OSK-Ophiolite) in northwestern Iran. The OSK-Ophiolite is known as the Neotethys, an ocean remnant in northwestern Iran, and extends to eastern Turkey and surrounds the Van area. This configuration shows that the Van microplate and surrounding ocean have played an important role in the evolution of magmatic activity in northwestern Iran, eastern Turkey, and the Caucasus since the Cretaceous. The Van microplate is situated among the Arabian plate to the south, northwestern Iran to the east, and Armenia to the north. The subduction of the northern branch of the Neotethys oceanic lithosphere beneath southern Eurasia has been critical in flare-up magmatism in the southern Caucasus since the Late Cretaceous. Considering the Van area as a new microplate makes understanding the geodynamic evolution of this area easier than in the many tectonic models that have been suggested before. When regarding the Van microplate, the main suture zone, which is known as the Bitlis–Zagros zone, should be changed to the Zagros–Khoy–Sevan–Akera suture zone, which extends to the eastern and northern Van microplate and western Iran.

Keywords: Van microplate, neotethys, Jurassic drifting, tethys ophiolites, NW Iran

OPEN ACCESS

Edited by:
Mei-Fu Zhou,
The University of Hong Kong, Hong Kong

Reviewed by:
Simone Tommasini,
University of Florence, Italy
Justin L. Payne,
University of South Australia, Australia

***Correspondence:**
Hossein Azizi
azizi1345@gmail.com
h.azizi@uok.ac.ir

Specialty section:
This article was submitted to Petrology, a section of the journal Frontiers in Earth Science

Received: *19 June 2020*
Accepted: *21 December 2020*
Published: *29 January 2021*

Citation:
Azizi H and Tsuboi M (2021) The Van Microplate: A New Microcontinent at the Junction of Iran, Turkey, and Armenia. Front. Earth Sci. 8:574385. doi: 10.3389/feart.2020.574385

INTRODUCTION

Most crust in Iran and Turkey is part of the Alpine–Himalaya orogenic belt, which is situated at the junction of Gondwana (in the south) and the Eurasian plate (in the north) (Dewey et al., 1973; An and Harrison, 2000; Göncüoglu, 2010; Prelević and Seghedi, 2013; Tian et al., 2017). This crust includes a number of microcontinents, such as the Taurides–Anatolides and Biston–Avoramanm, Bilitis, and Van microcontinents, with the latter being added by the authors in this research (**Figure 1**). These microcontinents were distributed across the Tethys Ocean in the Mesozoic to early Cenozoic eras but are now surrounded by oceanic-crust remnants (Jassim and Goff, 2006). Nevertheless, there is no well-defined information to confirm that these microcontinents completely drifted from the Arabian plate (Wrobel-Daveau et al., 2010; Azizi et al., 2013; Nouri et al., 2016).

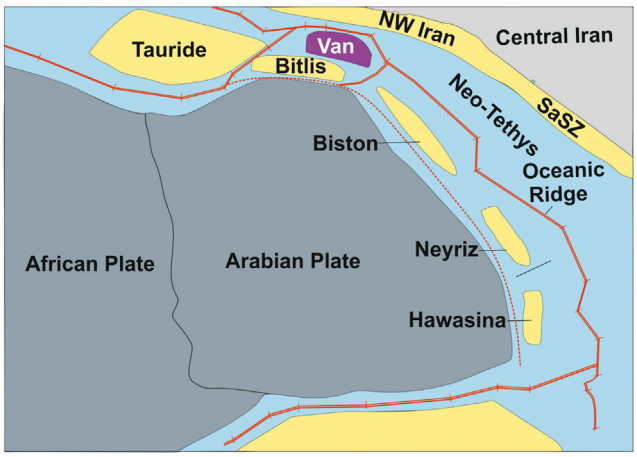

FIGURE 1 | Paleogeographic maps during the Late Jurassic-Early Cretaceous (Jassim and Goff, 2006) show that the Neotethys Ocean surrounded some microcontinents, such as Taurides–Anatolides and Biston–Avoramanm, Bilitis, and Van microcontinents, which were added by the authors in this research.

The northern fossil remnant of oceanic crust is known as the Paleo–Tethys trace, which extends from northern Iran to northern Turkey (Kroner and Romer, 2013; Manafi et al., 2013; Shafaii Moghadam and Stern, 2014). The central and southern parts (**Figure 2**) are known as the Neotethys remnant (Stöcklin and Nabavi, 1973; Golonka, 2004; Ghasemi and Talbot, 2006; Moghadam and Stern, 2015; Hassanzadeh and Wernicke, 2016; Nouri et al., 2019).

Magmatic activity increased in both northwestern Iran and Turkey in the Late Cretaceous and has continued through the Quaternary (Alavi, 1994). Magmatism in both regions was concentrated in four main periods: The Late Cretaceous, Eocene, Miocene, and Quaternary. According to many published research studies, most of the magmatic activity was related to the Tethys (Neotethys) orogeny, which stemmed from the subduction and collision of the Arabian plate with the Turkey and Iran plates, as well as from postcollisional tectonic regimes (Agard et al., 2006; Agard et al., 2011; Ali et al., 2013; Whitechurch et al., 2013; Nouri et al., 2016; Nouri et al., 2017; Nouri et al., 2020; Azizi et al., 2018b; Shabanian et al., 2018). Certainly, in Turkey and the western and central parts of Iran, magmatic rocks show clear similarities to the typical calc-alkaline, magmatic series common to an active continental margin (Parlak et al., 2000; Aldanmaz, 2006; Dilek and Altunkaynak, 2009; Topuz et al., 2004; Topuz et al., 2017).

The focus of this study is on magmatic activity in the region between the Black and Caspian Seas, which includes northwestern Iran, eastern Turkey, Georgia, Armenia, and Azerbaijan (**Figure 2**). This magmatism is of interest, as it has traditionally been considered to be a result of the subduction of oceanic crust of the Neotethys beneath Iran and southern Turkey. The site of this margin is considered to be represented by the

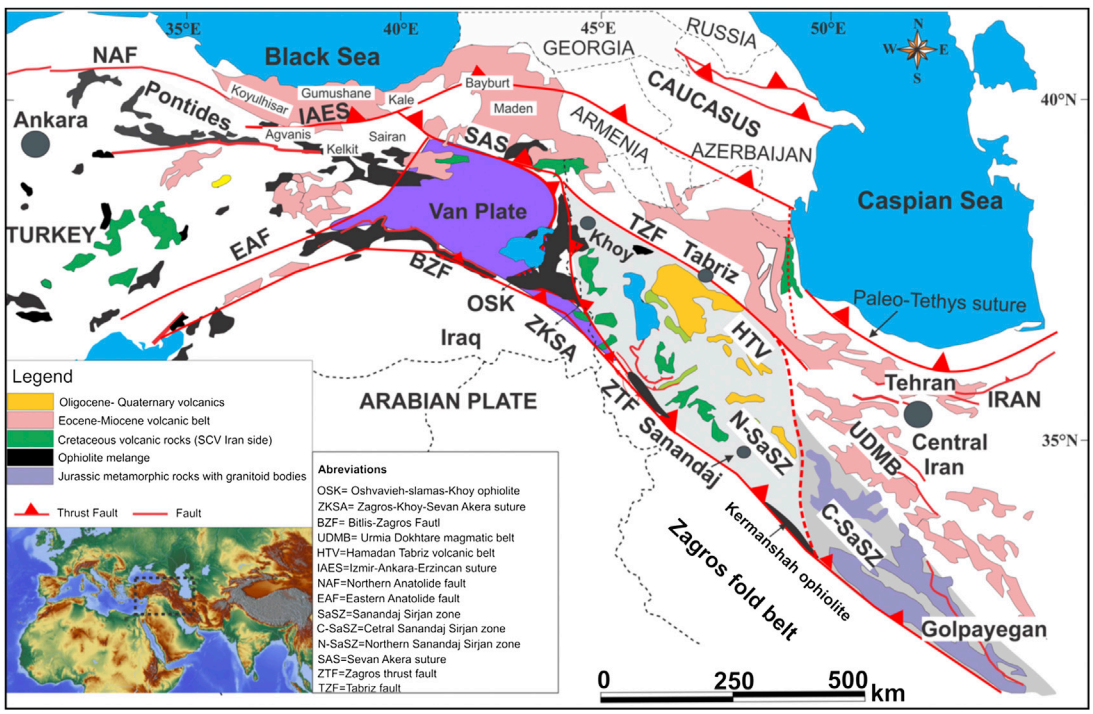

FIGURE 2 | Distribution of the main suture zones and magmatic rocks from the Cretaceous to Quaternary in Turkey and northwestern Iran with the Van-microplate position. Ophiolite members are distributed in the main suture zones that surround the Van microplate (modified from Nouri et al., 2016).

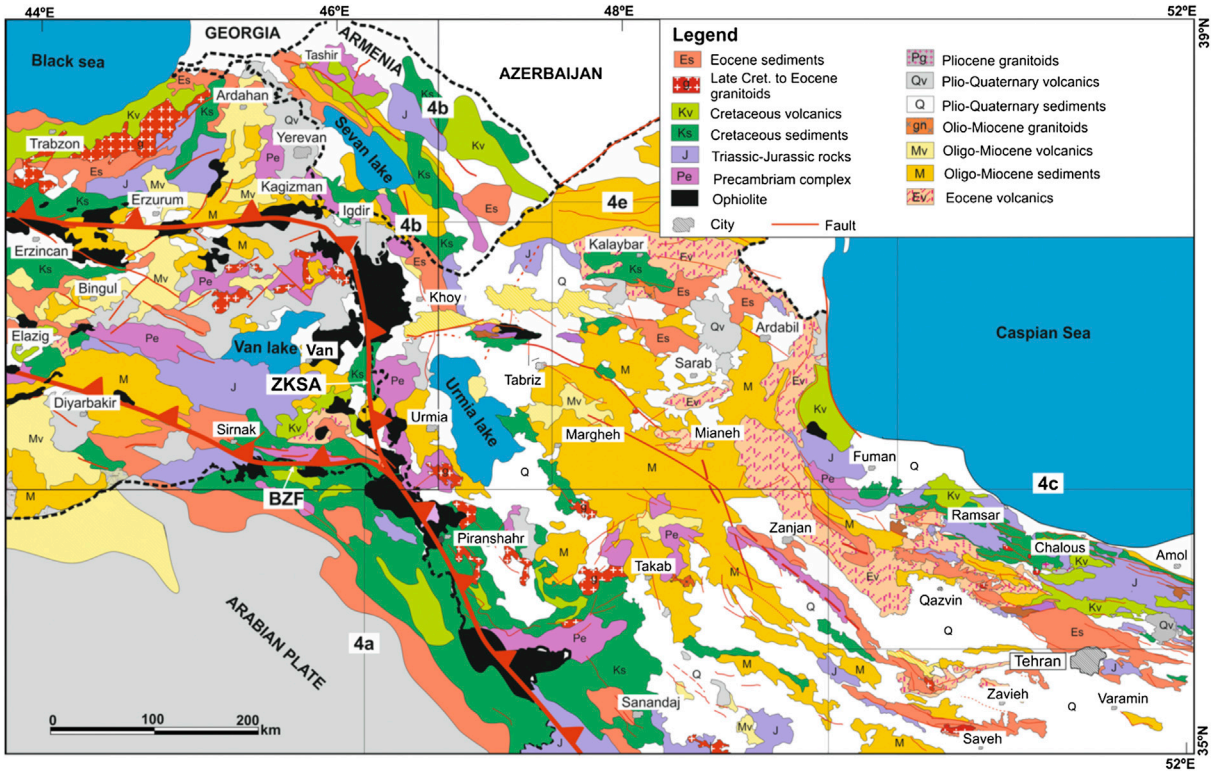

FIGURE 3 | Simplified geology units between the Black and Caspian seas that show the main sutures, ophiolites, and magmatic rocks in more detail. See the **Supplementary S1** for the references. Rectangles show the locations of the detailed geological maps in **Figure 4(A–E)** and the location of the study area examined by researchers.

Bitlis–Zagros–Fault (BZF) suture zone (**Figures 2**, **3**). As the BZF suture zone is distant from the southern and western Caspian Sea (>300 km), it is problematic for the highly, calc-alkaline magmatism to be sourced from subduction coming from that area. Furthermore, the location of the Khoy ophiolite sequence would appear to be inconsistent with subduction focused solely along the BZF. The large size of the Khoy ophiolite and its composition of pelagic sediment, a large thickness of pillow lava, sheeted dikes, both layered and massive gabbro, and cumulate and tectonite peridotites, are highly consistent with typical ophiolite sequences (Hassanipak and Ghazi, 2000; Ghazi et al., 2003; Khalatbari-Jafari et al., 2003) that have been generated in a mature, oceanic basin. These seeming inconsistencies in the geological record led us to propose the existence of a new microcontinent or continental fragment that sits between the BZF suture zone to the south and the Khoy ophiolite sequence to the northeast.

In this study, we introduce a new microplate, the Van microplate, which has an area of approximately 50,000 km^2 and is situated between northwestern and central Iran, the Anatolian block, and the Arabian plate (**Figure 3**). We outline and explain the proposed, microplate boundaries, followed by an explanation of how the northern branch of the Neotethys has controlled the magmatic activity of northwestern Iran and the Caucasus, based on this new microplate, despite the southern branch.

GEOLOGICAL BACKGROUND

Eocene volcanic rocks are widely distributed from the southern Caspian Sea to the southern Black Sea and are almost parallel to the Cretaceous volcanic rocks (**Figures 2**, **3**). **Figures 2**, **3** were compiled based on more than 20 geology maps of Iran and the surrounding area (See the **Supplementary S1** for the map references). Cretaceous volcanic rocks are also extensive, although less so in comparison to the Eocene rocks (**Figures 2**, **3**), and are limited to the south of the Zagros fault in the northern Sanandaj–Sirjan zone (SaSZ). Cretaceous magmatism primarily has calc-alkaline affinity (Azizi and Jahangiri, 2008; Azizi and Moinevaziri, 2009). Ophiolite members, known as Neotethys remnants, are widely distributed along major faults, such as the BZF and Zagros thrust-fault (ZTF) suture in southern Turkey and western Iran. The Bitlis–Zagros, which includes the BZF and ZTF here (**Figures 2**, **3**), is known as a major suture zone between the Arabian and Iranian–Anatolian plates. It was opened in the late Paleozoic Era and closed in the Cenozoic Era (Agard et al., 2011; Alirezaei and Hassanzadeh, 2012; Abdulzahra et al., 2016; Azizi et al., 2019).

Some dismembered mafic and ultramafic rocks are exposed throughout the entire Bitlis-Zagros suture zone in the border between Iran and Iraq along the BZF (**Figures 2**, **3**). Some researchers considered this complex as ophiolites

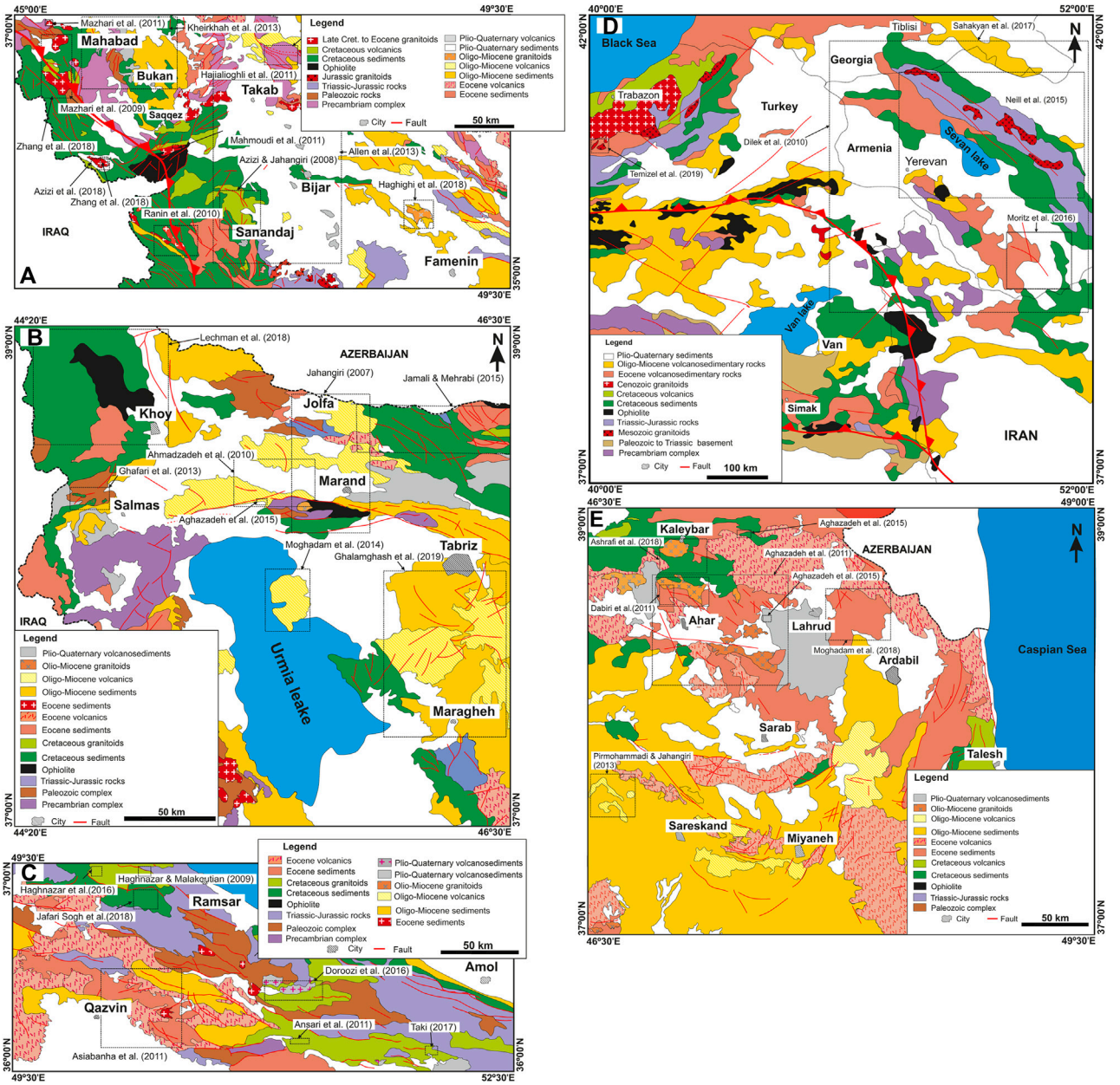

FIGURE 4 | (A–E) Detailed geological maps of the main magmatic units and major faults distributed between the Black and Caspian Seas. The location of collected data and references are shown in the maps. For the location of each map, see **Figure 3**.

(Ismail et al., 2010; Ali et al., 2013; Ali et al., 2016; Mohammad, 2013; Mohammad and Cornell, 2017; Al Humadi et al., 2019) and found that these rocks are more consistent with plume-type magma and barren rifts (Wrobel-Daveau et al., 2010; Azizi et al., 2013; Azizi and Stern, 2019; Karim and Al-Bidry, 2020). In this case, a barren rift between the Van microplate and Arabian plate is more likely than mature oceanic crust. These mafic rocks define the Sanandaj–Sirjan zone (SaSZ) from the Arabian plate in northwestern Iran to southern Turkey. The distribution of the magmatic rocks with the major faults from eastern Turkey to northern Iran is detailed in **Figures 4A–E**.

Azizi and Stern (2019) divided the SaSZ in western Iran (**Figure 2**) into three main parts: northern, central, and southern. In the northern part, which is separated from the Van microplate in this study and the junction, some dismembered ophiolite has been exposed. We call this the Oshnavieh-Salmas-Khoy ophiolite belt (OSK-Ophiolites) here. The OSK-Ophiolites, which has a N-S trend, is the main suture zone between the Van microplate and northwestern Iran block. We describe the OSK-Ophiolites below.

OSK Ophiolites

This dismembered ophiolite belt is exposed in a number of locations. It mainly shows mid-ocean ridge and island-arc, geochemical signatures and is widely exposed in the Khoy area, with some massive-sulfide mineralization and chromite deposits (Zaeimnia et al., 2017). In the Khoy area, the ophiolite members in the east have been classified as the main ultramafic parts of the mantle and comprise dunite and harzburgite (Khalatbari-Jafari et al., 2003). In the west, the members comprise oceanic crust, which consists of deep pelagic sediment, pillow lava, and sheeted dikes, all with a Cretaceous age. This complex was thrust onto the western side of the Van microplate, and the Precambrian basement (Azizi et al., 2011) was thrust onto the ultramafic complex on the eastern side. The entire complex was unconformably covered by Oligocene–Miocene conglomerate and a terrigenous sedimentary layer. The Khoy ophiolite sequences are typical of mid-ocean ridges in mature oceanic crust, such as the recent Pacific oceanic ridge (Sclater et al., 1971; Zhang et al., 2020).

Magmatic Activity

Magmatic activity around the Van microplate is restricted to four main intervals:

Cretaceous, Eocene, Oligocene-Miocene, and late Miocene-Quaternary.

Cretaceous Volcanic Rocks

Cretaceous volcanic rocks surrounding the Van microplate are mostly less exposed, being buried under younger sedimentary and volcanic rocks (**Figures 3**, **4**). Cretaceous volcanic rocks are mainly interbedded with sedimentary layers and are mainly basaltic and andesitic-basaltic rocks (Azizi and Jahangiri, 2008) that have erupted in submarine environments. Due to the high levels of alteration within these rocks, there have been few studies on these rocks. Whole-rock composition confirms that these rocks were formed in an active, continental margin (Azizi and Jahangiri, 2008).

Eocene Volcanic Rocks

This group of rocks is the main volcanic suit and extends from the western Caspian Sea to Armenia, Georgia, and northern Turkey (**Figures 3**, **4**). On the Turkish side, it is divided into two main extensions. The first part extends to the northern IAES fault, and the second extends in a NE-SW direction along the eastern Anatolian fault (EAF), which we consider to be the western edge of the Van microplate (**Figures 2–4**).

Oligocene–Miocene Magmatic Rocks

These volcanic and plutonic rocks are widely distributed, and they cut the Eocene volcanic rocks. Mainly Cu–Mo–Au deposits and Fe mineralization (Azizi et al., 2009; Siani et al., 2015; Mehrabi et al., 2016; Rabiee et al., 2019) occurred during magmatic activity in the western and southern areas of the Caspian Sea.

Late Miocene-Quaternary Rocks

This group of rocks is distributed along the rim of the Van microplate, and they are classified into two main groups. The first group includes adakite and adakitic rocks, and the second includes high-Nb, basaltic rocks (Jahangiri, 2007; Azizi et al., 2014a; Azizi et al., 2014b), which confirms that they were formed in a postcollisional, tectonic regime. In addition, some of the major Pliocene-Quaternary volcanoes, such as Sahand, Sabalan, and Ararat, erupted at this time (Allen et al., 2013a; Chiu et al., 2013; Ghalamghash et al., 2019).

WHOLE-ROCK CHEMISTRY

We have compiled whole-rock, chemical data on 900 volcanic rocks (Agostini et al., 2007; Jahangiri, 2007; Azizi and Jahangiri, 2008; Haghnazar and Malakotian, 2009; Mazhari et al., 2009, 2011; Ahmadzadeh et al., 2010; Dilek et al., 2010; Ranin et al., 2010; Aghazadeh et al., 2011; Aghazadeh et al., 2015; Ansari et al., 2011; Dabiri et al., 2011; Hajialioghli et al., 2011; Mahmoudi et al., 2011; Asiabanha and Foden, 2012; Alishah et al., 2013; Ansari, 2013; Castro et al., 2013; Ghaffari et al., 2013; Kheirkhah et al., 2013; Moghadam et al., 2014; Neill et al., 2015; Doroozi et al., 2016; Haghnazar et al., 2016; Moritz et al., 2016; Sahakyan et al., 2017; Taki, 2017; Ashrafi et al., 2018; Haghighi Bardineh et al., 2018; Jafari Sough et al., 2018; Lechmann et al., 2018; Shafaii Moghadam et al., 2018; Zhang et al., 2018; Azizi et al., 2019; Ghalamghash et al., 2019; Temizel et al., 2019) from Cretaceous to Quaternary magmatism in northwestern Iran, southern Armenia, and eastern Turkey (**Supplementary S2**). The sample locations and references for each area are shown in **Figures 4A–E**.

Cretaceous volcanic rocks include basalt to rhyolite but are mostly classified as andesite. Cretaceous intrusive bodies also show some variation from gabbro to granite, with less exposure compared to volcanic rocks. Whole-rock composition shows that the Cretaceous, magmatic rocks have a large variation in TiO_2 from 0.19 to 3.82 wt% (average = 1.52 wt%, n = 125), Al_2O_3 from 11.2 to 22.7 wt % (average = 15.9 wt%, n = 125), and MgO from 0.03 to 11.8 wt% (average = 5.27 wt%, n = 125). In addition, these rocks have a high concentration of Ba (average = 470 ppm, n = 125), U (average = 2.82 ppm), and Th (average = 8.9 ppm). Eocene–Miocene, magmatic rocks have a large variation in SiO_2 (43–77 wt%), high content of Rb (average = 100 ppm; n = 389), Sr (average = 618 ppm, n = 429), Th (average = 11.7 ppm, n = 331) and U (3.47 ppm, n = 341). The upper Miocene-Quaternary magmatic rocks are mostly categorized into two main groups: adakite, with higher ratios of Sr/Y and La/Yb; and alkali basalts, with a higher content of Nb (average = 27 ppm, n = 328). See **Supplementary S2** for more information about the whole-rock chemistry of each group. For our discussion, the samples are categorized into three main groups: Cretaceous, Eocene-Miocene, and upper Miocene-Quaternary. All of the groups show variances from the basalt to the rhyolites (**Figure 5**) in the $K_2O + Na_2O$ diagrams (Le Bas et al., 1986). Nevertheless, the alkali elements for the Cretaceous and Eocene magmatic rocks largely varied compared to the upper Miocene and Quaternary rocks.

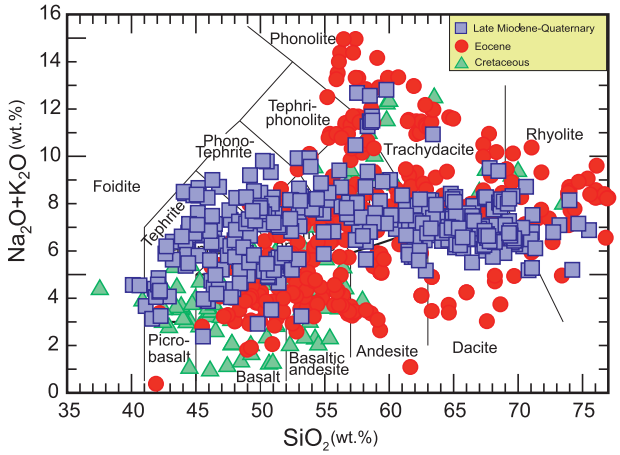

FIGURE 5 | Distribution of the composition of whole rocks, from Cretaceous to Quaternary, for all igneous rocks situated in the southern and western Caspian Sea. For references, see the text and **Supplementary S2**.

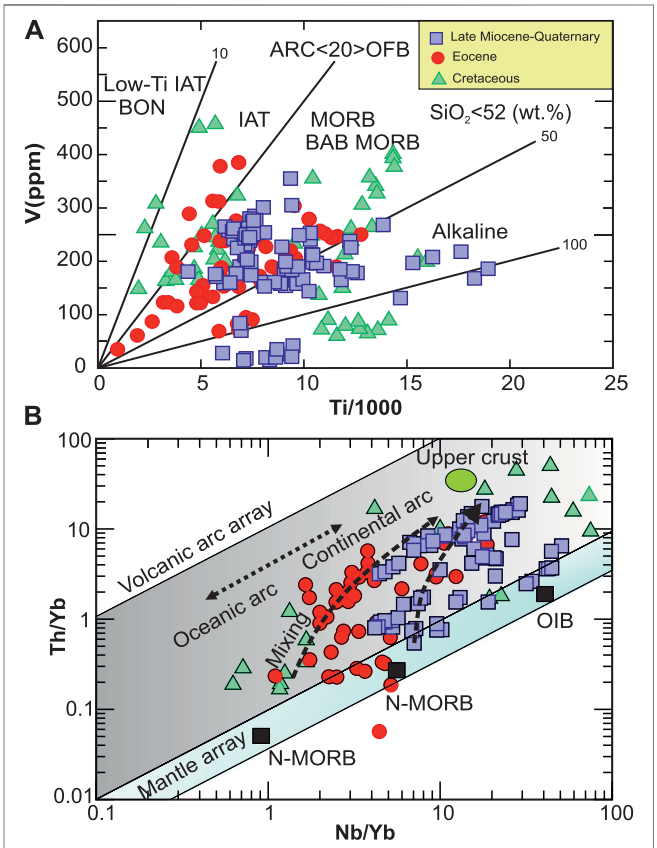

FIGURE 6 | Distribution of basic rocks (SiO_2 less than 52 wt%) from the southern and western Caspian Sea with different ages from the Cretaceous to Quaternary in the Ti–V Diagram (Shervais, 1982) and Th/Yb vs. the Nb/Yb diagrams (Pearce, 2008) in a and b, respectively. The mafic rocks plot near the arc and back-arc fields in the Ti–V diagram, and the higher ratios of the Th/Yb ratios plot in the volcanic-arc field in the Nb/Yb-Th/Yb ratios. See the text for more information and references for the data. For source data, see **Supplementary S2**. *Abbreviations: MORB = Mid-Oceanic Ridge Basalt; BAB = Back Arc Basalt; IAT = Island Arc tholeiite; BON = Boninite.*

TECTONIC SETTING

For understanding tectonic setting, some key and general petrological diagrams are briefly used here. The Ti/V ratio diagram (Shervais, 1982) shows a wide distribution of the Cretaceous volcanic rocks from the arc to extensional basins (**Figure 6A**). Eocene rocks have more affinities for the arc-magma series. The late Miocene-Quaternary arc affinity was decreased and extended to alkaline and within-plate series (**Figure 6A**). The Th/Yb vs. Nb/Yb diagram (Pearce, 2008) shows that most of the mafic rocks plot in the volcanic-arc field because of the higher ratios of Th/Yb (**Figure 6B**). The enrichment of Th occurred during the fluids released from the subduction of the oceanic crust and/or crustal contamination with some assimilation-fractionation and contamination (AFC) processes. The Cretaceous basaltic rocks show a dichotomy for both intraoceanic arc and active continental-tectonic regimes. Eocene basaltic rocks show a clear relation to the typical active continental margin. Upper Miocene-Quaternary basaltic rocks also plot in the volcanic-arc field, with some similarity to oceanic-island basaltic rocks (OIB) near the mantle array, with less effect on crustal components (**Figure 6B**). To avoid the mobility of some trace elements, all Eocene and younger basaltic rocks, other than Cretaceous volcanic rocks because of the wide ranges, were normalized using rare-earth elements (REEs) of the chondrite value (Sun and McDonough, 1989). The normalized pattern shows that both the Eocene and upper Miocene-Quaternary rocks have higher ratios of light REEs than heavy REEs, and negative slopes from LREEs to HREEs (**Figures 7A,B**). Furthermore, the REE_S contained in the upper Miocene-Quaternary rocks are higher than those in the Eocene basaltic rocks (**Figures 7A,B**).

The plotting of the intermediate-to-acidic rocks (SiO_2 > 52 wt%) in FeO/(FeO + MgO) and $Na_2O + K_2O$–CaO vs. SiO_2 (Frost et al., 2001) shows that the lower ratios of FeO/(FeO + MgO) for most of the samples from the three groups plot in the magnesian and/or I–type granite fields. Some of the Cretaceous and Eocene samples extend to the ferroan granite field. The upper Miocene-Quaternary rocks mainly plot in the magnesian field and/or I-type granite area (**Figure 8A**). In the $Na_2O + K_2O$–CaO vs. SiO_2 (wt%), Cretaceous and Eocene samples are scattered from the calcic to alkalic fields. Nevertheless, most of the samples were concentrated in the alkali-calcic field. The upper Miocene-Quaternary rocks plot in the alkali-calcic field, with less variation than the Cretaceous and Eocene samples (**Figure 8B**).

Intermediate-to-acidic rocks (SiO_2 > 52 wt%) have higher ratios of Rb; lower ratios of Y, Ta, and Nb (**Figures 9A,B**); and almost plot in the active margin to within-plate domains (Pearce et al., 1984). Cretaceous intermediate-to-acidic volcanic rocks mainly plot in the active margin and within-plate tectonic fields. The variation in the Ta/Yb vs. Th/Yb ratios (Pearce, 1982) shows a wide range for the Eocene and Cretaceous intermediate-to-acidic magmatic rocks and more affinity with the upper Miocene-Quaternary for the within-plate granite field (**Figure 9C**).

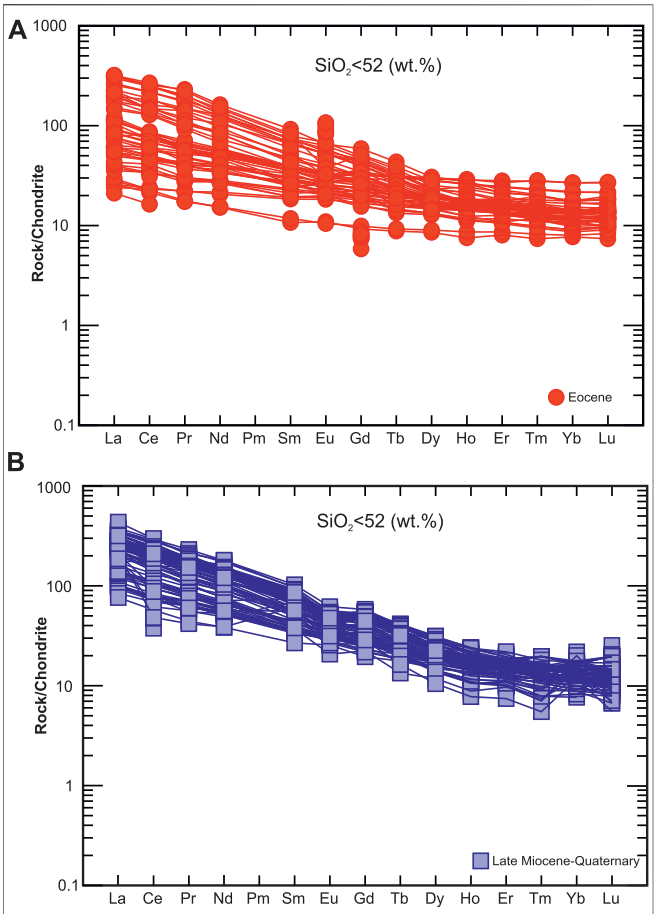

FIGURE 7 | Normalized REE abundances of the Eocene **(A)** and upper Miocene-Quaternary basic rocks (SiO_2<52 wt%) with chondrite values (Sun and McDonough, 1989). The normalized pattern shows that both the Eocene and upper Miocene-Quaternary rocks have higher ratios of light REEs than heavy REEs and negative slopes from LREEs to HREEs.

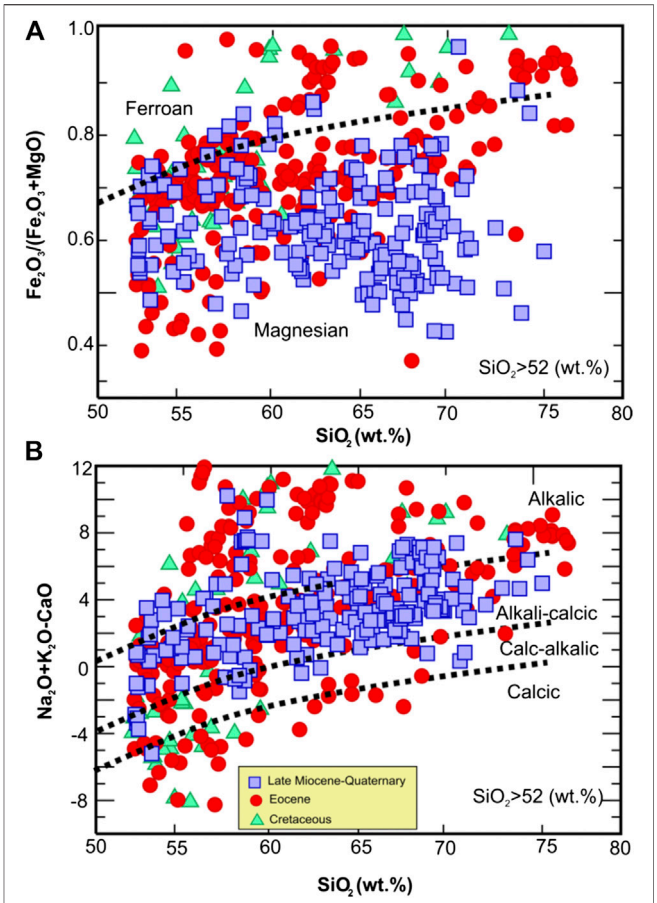

FIGURE 8 | Plotting of the intermediate to acidic rocks in the FeO/(FeO + MgO) vs. SiO_2 **(A)** and $Na_2O + K_2O$-CaO vs. SiO_2 (Frost et al., 2001) diagrams **(B)**, which are used for intermediate and acidic rock classification. See the text for more information.

The scattering of the Cretaceous volcanic rocks probably supports different tectonic regimes during the Cretaceous and requires more detailed work because the Cretaceous volcanic rocks were strongly altered by seawater reactions. Some parts of intermediate-to-acidic rocks have higher ratios of Sr/Y and La/Yb and, based on the adakite key diagrams (Defant and Drummond, 1990), are classified as adakite (**Figure 10A**). The high affinity of the upper Miocene-–Quaternary volcanic rocks for adakite groups, as well as the accompanying high-Nb basaltic rocks, means that there is a correspondence to a postcollisional tectonic regime in northwestern Iran since the Miocene (Azizi et al., 2014a; Asiabanha et al., 2018; Torkian et al., 2019).

Sr-Nd ISOTOPE RATIOS

We plotted 203 sample data points (**Supplementary S2**) in the $^{87}Sr/^{86}Sr$ vs. $^{143}Nd/^{144}Nd$ diagram collected from published works (Alpaslan et al., 2004; Agostini et al., 2007; Haghnazar and Malakotian, 2009; Mazhari et al., 2009, Mazhari et al., 2011; Aghazadeh et al., 2011, Aghazadeh et al., 2015; Dabiri et al., 2011; Allen et al., 2013a, Allen et al., 2013b; Ghaffari et al., 2013; Moghadam et al., 2014; Neill et al., 2015; Sahakyan et al., 2017; Haghighi Bardineh et al., 2018; Lechmann et al., 2018; Shafaii Moghadam et al., 2018; Azizi et al., 2019). Most samples plot near the mantle array with some variation for the Cretaceous and Eocene igneous rocks. Cretaceous samples plot in two main areas: the first group plots near the cross lines of the chondrite uniform reservoir (CHUR) and bulk silicate earth (BSE); and the second group, with lower ratios of $^{143}Nd/^{144}Nd$ and higher ratios of the $^{87}Sr/^{86}Sr$, plots with the combination of both mantle and crustal components for the evolution of these rocks (**Figure 11**).

Eocene igneous rocks mainly plot in the depleted-mantle area and extend to the lower $^{143}Nd/^{144}Nd$ ratio and higher $^{87}Sr/^{86}Sr$ ratio fields, which show heterogeneous sources such as depleted mantle and primitive and metasomatized mantle for the sources of these rocks. Furthermore, the scattering of Eocene samples in the $^{87}Sr/^{86}Sr$-$^{143}Nd/^{144}Nd$ diagram suggests the involvement of both mantle material and crustal components in the magmatic

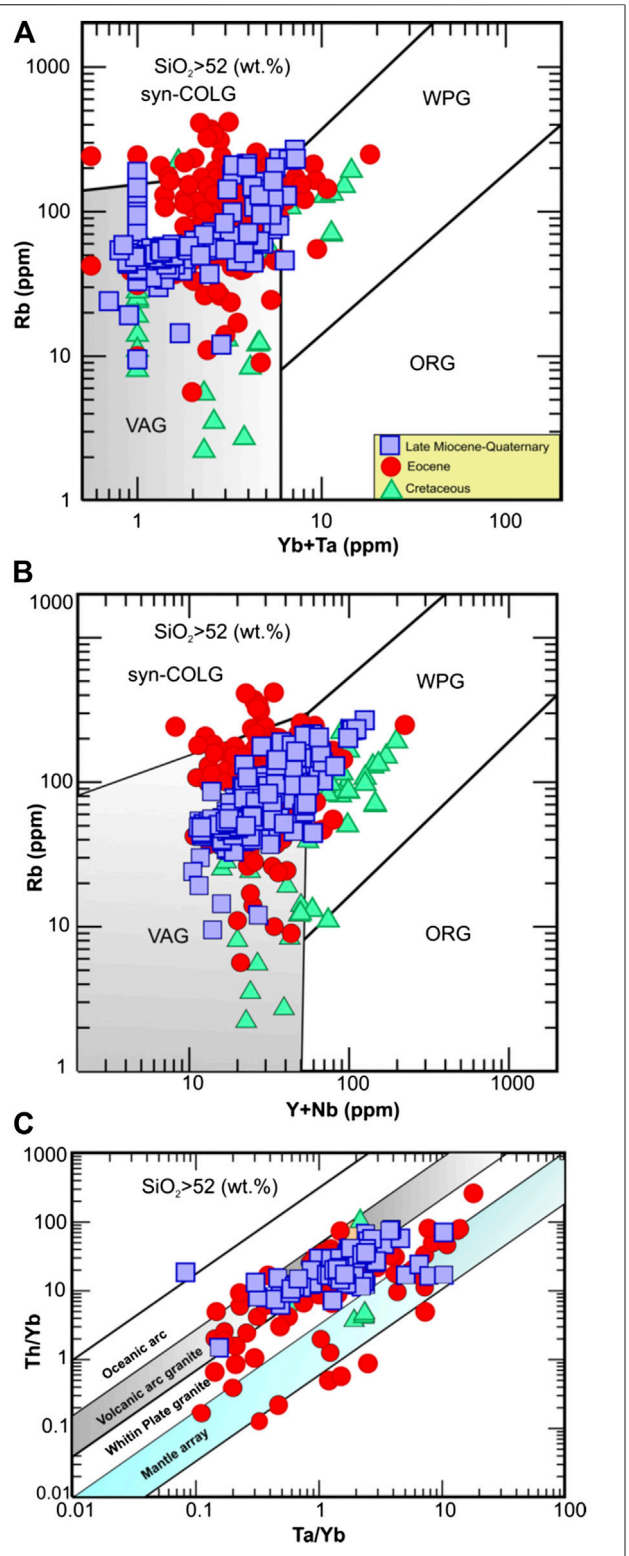

FIGURE 9 | Intermediate to acidic rocks (SiO_2 > 52 wt%) of the Eocene and Miocene mainly plot in the volcanic-arc, tectonic regime, whereas Cretaceous rocks plot in the arc and within-plate fields in the Rb–Yb + Ta **(A)** and Rb–Y + Nb **(B)** diagrams (Pearce et al., 1984). The variation in the Ta/Yb vs. the Th/Yb ratios (Pearce, 1982) shows a wide range for the Eocene

(*Continued*)

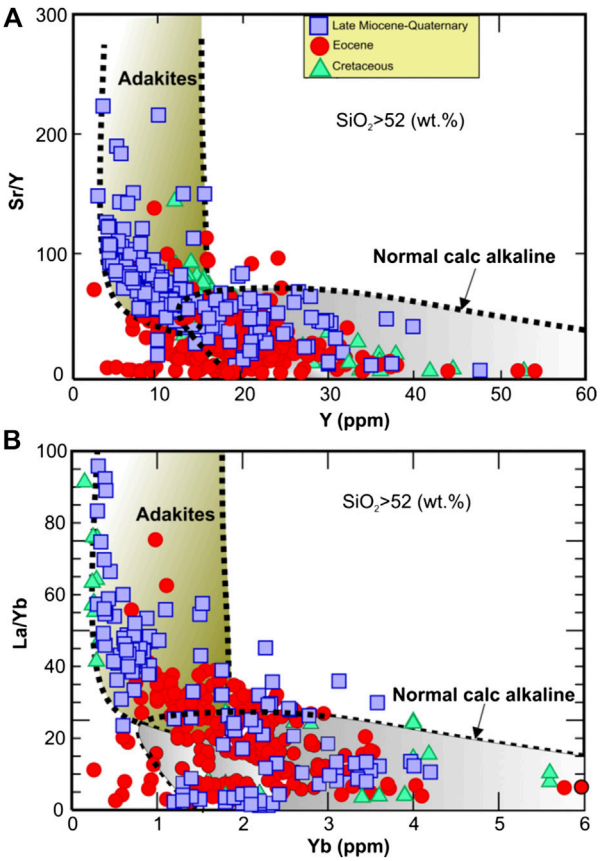

FIGURE 10 | Some intermediate-to-acidic rocks have higher ratios of Sr/Y and La/Yb and are classified as adakite **(A and B)**. See the text for more information. For source data and references, see **Supplementary S2**.

activity during the Eocene. The scattering of the Sr–Nd isotope ratios shows three main trends for the evolution of the Eocene magmatic rocks, which we call EO.1, EO.2, and EO.3 (**Figure 11**). These three trends show depleted mantle with higher ratios of $^{143}Nd/^{144}Nd$ (>0.51290), such as from the subcontinental-lithospheric mantle, as the primary source. During magmatic evolution and/or later, they have been affected by crustal components (EO.2 and EO.3 trend) and/or alteration (EO.1 trend). Due to the wide distribution of Eocene volcanism and the variation in Sr-Nd isotope ratios, metasomatized mantle from the oceanic slab is also the main alternative for the genesis of these rocks, which has been suggested by many researchers for the sources of these rocks.

Upper Miocene to Quaternary samples plot near the mantle array from the depleted mantle to enriched mantle in the $^{87}Sr/$

FIGURE 9 | intermediate-to-acidic rocks and more affinity of the upper Miocene–Quaternary for the within-plate field **(C)**. For source data and references, see **Supplementary S2**. *Abbreviations: MORB = Mid-Oceanic Ridge Basalt; BAB = Back Arc Basalt; IAT = Island Arc tholeiite; BON = Boninite; COLG = Collision Granite; VAG = Volcanic Arc Granite; ORG = Oceanic Ridge Granite; WPG= Within-Plate Granite.*

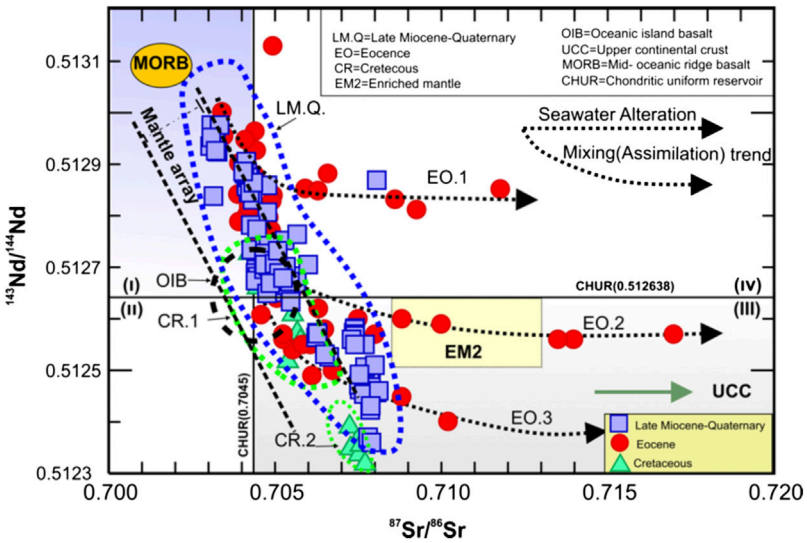

FIGURE 11 | Distribution of $^{87}Sr/^{86}Sr$ vs. $^{143}Nd/^{144}Nd$ ratios shows that the main samples extend along mantle arrays. The Cretaceous samples are plotted in two different fields, CR.1 and CR.2. The Eocene rocks show three different patterns—EO1-EO3—which confirms some seawater alteration and continental-crustal mixing. Upper Miocene-Quaternary samples plot in mantle arrays with less variation. For the sources of the data, see **Supplementary S2**.

^{86}Sr–$^{143}Nd/^{144}Nd$ ratio diagram (**Figure 11**). Most samples are concentrated near the cross line of the CHUR, which mainly shows the combination of depleted ($^{143}Nd/^{144}Nd > 0.512638$) to primitive mantles ($^{143}Nd/^{144}Nd = 0.512638$) as the main sources of these rocks. Crustal-component interactions, for example, assimilation with the magma, are lower than those of the Eocene magmatic rocks (**Figure 11**), which may suggest the thinning of the continental crust after collision. Therefore, depleted mantle, oceanic-island basalt (OIB), source-like, and enriched mantle (EM2) contributed to the genesis of Eocene and upper Miocene-Quaternary magmatic activity, with less contribution from continental crust for the upper Miocene-Quaternary rocks.

DISCUSSION

In most of the traditionally published research, the northern and eastern Bitlis–Zagros suture zone has been considered as an active continental margin since the Jurassic Period (Davoudian et al., 2008; Agard et al., 2011; Hassanzadeh and Wernicke, 2016). Recently published research has confirmed that the initiation of Neotethys subduction beneath the SaSZ (Azizi and Stern, 2019) occurred in the Cretaceous Period, and the collision of the Arabian plate and Van microplate in northwestern Iran occurred in the late Eocene epoch (Azizi et al., 2019). Nevertheless, there are some weak points concerning the relationship of ultramafic rocks to the ophiolite complex in northeastern Iraq within the suture of the Arabian plate and Van microplate. There is also no strong evidence for a typical ophiolite complex here (Azizi et al., 2013). In line with our suggestion, the new OSK zone shows that northwestern Iran-eastern Turkey magmatism was mainly controlled by Neotethys oceanic subduction, which was situated on the northern side of the Van microplate (**Figures 2**, **3**). The Khoy ophiolites mainly occurred during the Late Cretaceous Period (Ghazi et al., 2003; Khalatbari-Jafari et al., 2003, 2004; Moghadam and Stern, 2015) and are in contact with upper Neoproterozoic/lower Paleozoic granites (Azizi et al., 2011) in the east. Additionally, the Precambrian basements mainly include intrusive granite and metamorphic rocks, which were exposed in the Khoy, Urmia (Urmiah), and Tabriz areas. Northwestern Iran was obducted onto the east side of the OSK suture zone (**Figure 3**).

Tertiary volcanism surrounded the Van microplate (**Figures 2**, **3**). Meanwhile, distinct depression basins, such as the Urmia Lake basin (**Figures 2**, **3**), were formed near the OSK suture zone. All evidence shows a typical arc-type tectonic regime here. Nevertheless, our information on the Cretaceous magmatic rocks in northwestern Iran is not sufficient. The Neotethys ophiolite or ophiolite-like belt in northwestern Iran is divided into two branches in the area around Piranshahr (**Figure 3**). The southern (southwestern) branch extends to northeastern Iraq and continues to southern Bitlis, and it is known as the BZF suture zone here. This branch does not show a clear relationship to typical ophiolites, but it has some correlation with plume-type (Azizi et al., 2013) sources with some affinity for immature oceanic crust and/or continental rifts. The second branch is the OSK suture zone, which extends in a NW-SE direction in western Iran and joins the Sevan-Akera suture zone (SAS) in its northern part (**Figures 2**, **3**). The southern branch on the Iran side is named the Kermanshah-Nayriz ophiolites and is exposed along the Zagros fault in western Iran (**Figure 3**).

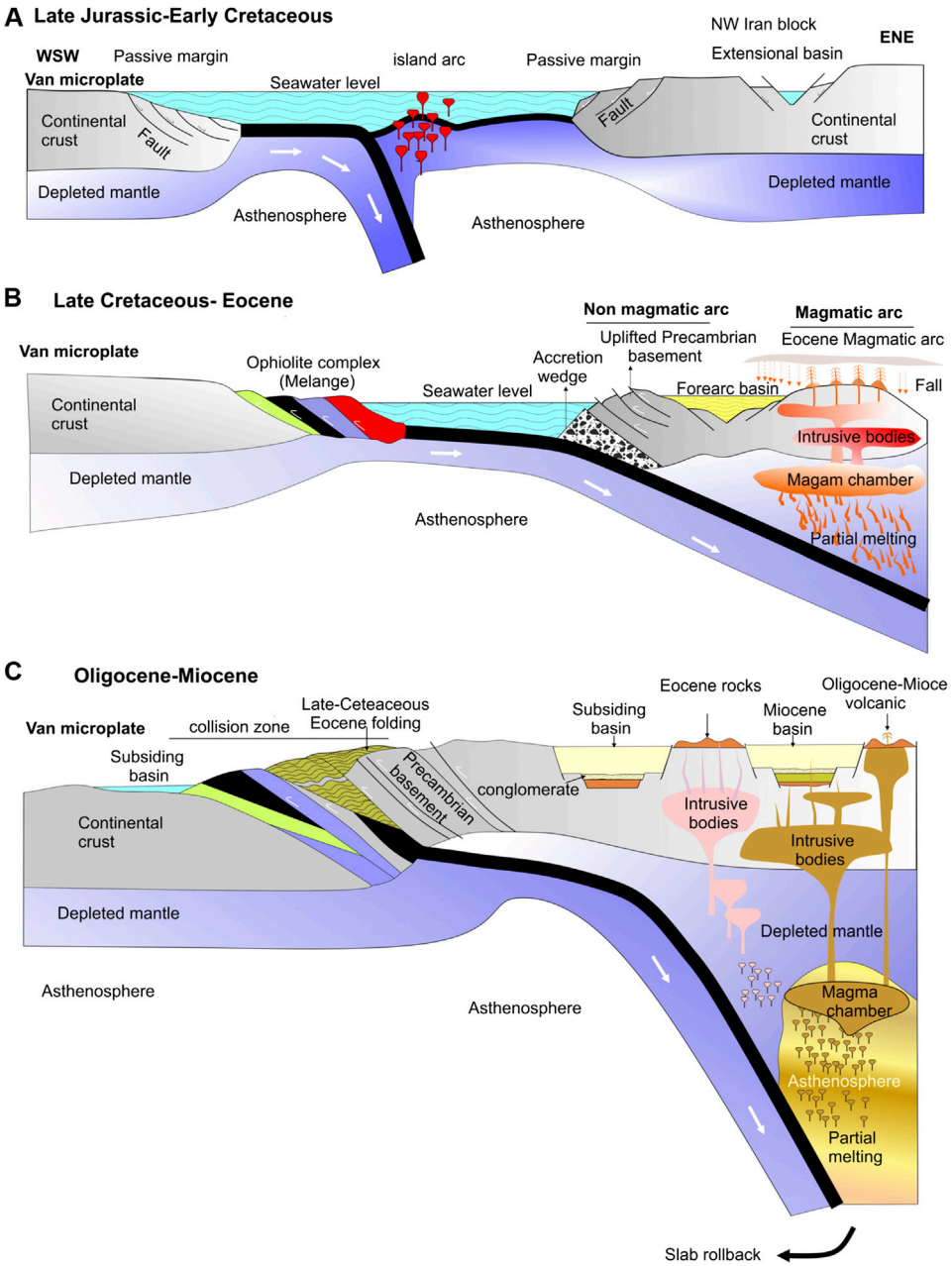

FIGURE 12 | Schematic tectonic model for the development of the magmatic arc from the Jurassic to the Oligocene-Miocene in the northwestern Iran block. **(A)** Development of the intraoceanic arc system in the Late Jurassic-Early Cretaceous periods. **(B)** Obduction of the Piranshahr-Khoy ophiolite complex over the Van microplate passive margin. Subduction of the northern branch of the Neotethys beneath the northern continent in the Late Cretaceous-Eocene led to the development of nonarc and arc magmatism and an Eocene forearc basin. **(C)** Collison of the Van microplate and NWIA, followed by the obduction of the Precambrian basement. Fragmentation of the Eocene magmatic belt, the development of interarc basins, injection, and the eruption of Miocene magmatic rocks. These processes occurred due to oceanic rollback after collision in the Oligocene-Miocene.

Magmatic activity since the Late Cretaceous Period developed in the northern and eastern parts of the Van microplate (**Figure 3**). The northern branches of the Neotethys, which were situated between the Van microplate to the south and the northwestern Iran-Armenia block (NWIA) to the north, were subducted beneath the NWIA block during the middle to Late Cretaceous Period. To consider the magmatic evolution in the southern rim of the NWIA, we suggest the following schematic model for the evolution of magmatic rocks in this belt since the Mesozoic.

Based on our suggested model, Jurassic rocks developed in the Van microplate. NWIA also probably shows the fragmentation of the Van microplate that occurred in the Late Jurassic/Early

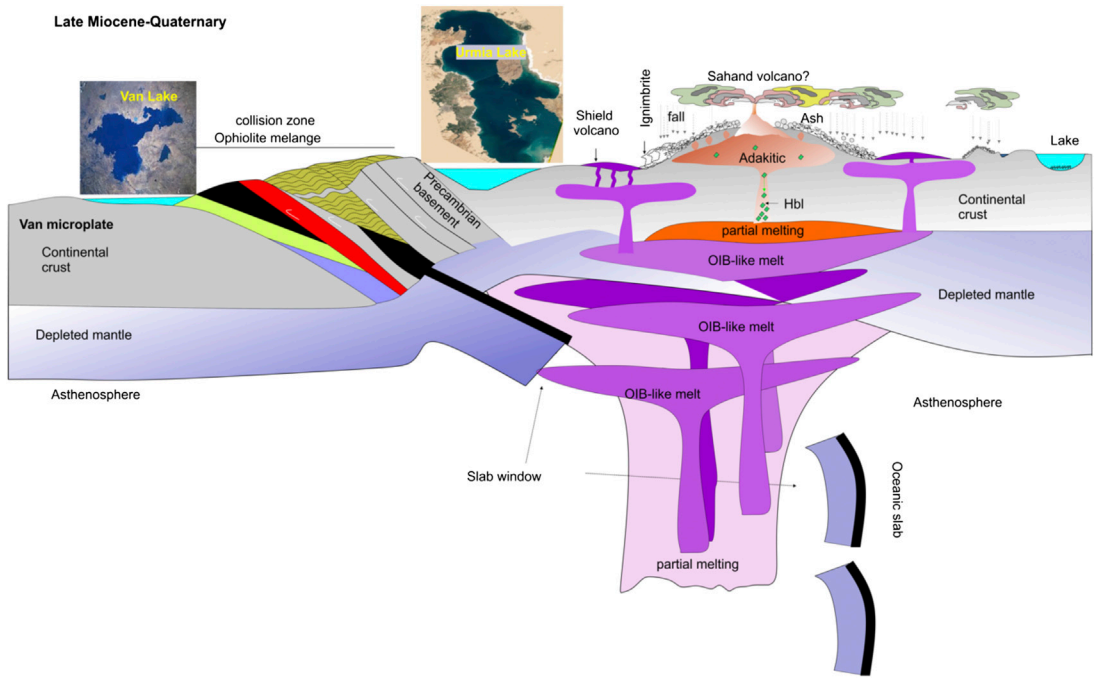

FIGURE 13 | Development of postorogenic basaltic-and-acidic volcanism during the Pliocene-Quaternary in northwestern Iran due to the slab window and injection of hot magma in the base of the lower crust, along with partial melting of earlier calc-alkaline bodies in the hot-root zone. Furthermore, during these processes, Van Lake as a foreland and Urmia Lake as a forearc basin were developed.

Cretaceous periods. Some evidence shows that the Jurassic magmatism was related to the extensional regime and continental rifts in the Khoy area (Khalatbari-Jafari et al., 2003; Lechmann et al., 2018; Miyazaki et al., 2018; Shafaii Moghadam et al., 2019), and they probably confirm the extensional regime or drifting of the Van microplate during the Cimmerian orogeny. This evidence is also consistent with the SaSZ tectonic regime, which had an extensional regime in the Middle-Late Jurassic Period (Azizi et al., 2018a; Badr et al., 2018; Azizi and Stern, 2019).

The OSK ophiolites have been thrust onto the passive margin and are overlaid by Paleocene sedimentary rocks. The ophiolite obduction on the passive margin probably occurred in a continental-arc collision system and, following the Neotethys, it started to subduct beneath the NWIA in the Late Cretaceous (**Figures 12A,B**). During subduction, nonarc magmatism, arc magmatism, and forearc basins developed in an active margin in the NWIA. Precambrian basements were obducted at this time (**Figures 12A,B**), and Upper Cretaceous-Eocene, magmatic rocks were produced during this process.

After colliding with the Van microplate and NWIA in the late Oligocene-Miocene, the oceanic crust experienced rollback, and the NWIA plate was overridden and affected by the extensional regime; some subsiding basins developed among the Eocene fragmented volcanic belt (**Figure 12C**). Deposition in the sedimentary basins started unconformably with a basal conglomerate on top of the Cretaceous-Eocene complex (**Figure 12C**). The extensional regime after the collision, the thinning of the NWIA, and the high-angle subduction connected both the lithospheric and asthenospheric mantle for the genesis of the magmatic rocks in the Miocene Epoch (**Figure 12C**). In the late stage, the oceanic crust was dismembered, and hot magma was injected from the slab window (**Figure 13**). Some parts of the magma erupted directly and made basaltic rocks that had a high similarity to the OIB composition in the HTV belt from Ararat to northern Sanandaj (Kheirkhah et al., 2009; Asiabanha and Foden, 2012; Azizi et al., 2014a; Torkian et al., 2016; Asiabanha et al., 2018). Other parts crystallized inside the lower crust and increased the geothermal gradient in the continental crust. This process was the basis for the partial melting of the lower crust and the production of adakite-like magma in the HTV belt during the Pliocene-Quaternary (Azizi et al., 2014b; Torkian et al., 2019).

CONCLUSION

This research shows that the Van microplate drifted from the Arabian plate in the Jurassic or earlier and is now surrounded by dismembered Neotethys ophiolite. During the closure of the northern branch of the Neotethys and the incorporation of the Van microplate into the southern Eurasian plate, a long period of magmatic activity (from the Late Cretaceous Period to the present) occurred along the southern rim of Eurasia, northwestern Iran, and the Caucasus. Therefore, the main suture is not Bitlis–Zagros, which has been suggested as the

junction of the Arabian and Iran-Armenia plates. Instead, it seems that Zagros–Khoy–Akera is the main suture zone, and it should be considered in future studies. The Zagers–Khoy–Akera suture can explain magmatism in the Caucasus and northwestern Iran more easily than the BZS. Furthermore, the northern SaSZ separated from the Anatolian plate via the Van microplate.

DATA AVAILABILITY STATEMENT

The original contributions presented in the study are included in the article/**Supplementary Material**, further inquiries can be directed to the corresponding author.

AUTHOR CONTRIBUTIONS

All authors listed have made a substantial, direct, and intellectual contribution to the work and approved it for publication.

FUNDING

This research was supported by the Japan Society for the Promotion of Science (JSPS) KAKENHI Grant No. 17H01671.

ACKNOWLEDGMENTS

This paper benefited greatly from previously published works, most of which we referred to in this work. We would like to thank F. Nouri for some technical support. This paper was greatly improved by three anonymous reviewers and the critical comments of the editor, Me-Fu Zhou.

SUPPLEMENTARY MATERIAL

The Supplementary Material for this article can be found online at: https://www.frontiersin.org/articles/10.3389/feart.2020.574385/full#supplementary-material.

REFERENCES

Abdulzahra, I. K., Hadi, A., Asahara, Y., Azizi, H., and Yamamoto, K. (2016). Zircon U–Pb ages and geochemistry of Devonian a-type granites in the Iraqi Zagros Suture Zone (Damamna area): new evidence for magmatic activity related to the Hercynian orogeny. *Lithos.* 264, 360–374. doi:10.1016/j.lithos.2016.09.006

Agard, P., Monié, P., Gerber, W., Omrani, J., Molinaro, M., Meyer, B., et al. (2006). Transient, synobduction exhumation of Zagros blueschists inferred from P–T, deformation, time, and kinematic constraints: implications for Neotethyan wedge dynamics. *J. Geophys. Res. Solid Earth.* 111, 4103. doi:10.1029/2005JB004103

Agard, P., Omrani, J., Jolivet, L., Whithechurch, H., Vrielynck, B., Spakman, W., et al. (2011). Zagros orogeny: a subduction-dominated process. *Geol. Mag.* 148, 692–725. doi:10.1017/S001675681100046X

Aghazadeh, M., Castro, A., Badrzadeh, Z., and Vogt, K. (2011). Post-collisional polycyclic plutonism from the Zagros hinterland: the Shaivar Dagh plutonic complex, Alborz belt, Iran. *Geol. Mag.* 148, 980–1008. doi:10.1017/S0016756811000380

Aghazadeh, M., Prelević, D., Badrzadeh, Z., Braschi, E., van den Bogaard, P., and Conticelli, S. (2015). Geochemistry, Sr–Nd–Pb isotopes and geochronology of amphibole- and mica-bearing lamprophyres in northwestern Iran: implications for mantle wedge heterogeneity in a palaeo-subduction zone. *Lithos.* 216–217, 352–369. doi:10.1016/j.lithos.2015.01.001

Agostini, S., Doglioni, C., Innocenti, F., Manetti, P., Tonarini, S., and Savasçin, M. Y. (2007). *The transition from subduction-related to intraplate Neogene magmatism in the Western Anatolia and Aegean area.* New York, NY: Special Papers-Geological Society of America.

Ahmadzadeh, G., Jahangiri, A., Lentz, D., and Mojtahedi, M. (2010). Petrogenesis of Plio-Quaternary post-collisional ultrapotassic volcanism in NW of Marand, NW Iran. *J. Asian Earth Sci.* 39, 37–50. doi:10.1016/j.jseaes.2010.02.008

Al Humadi, H., Väisänen, M., Ismail, S. A., Kara, J., O'Brien, H., Lahaye, Y., et al. (2019). U–Pb geochronology and Hf isotope data from the Late Cretaceous Mawat ophiolite, NE Iraq. *Heliyon.* 5, e02721. doi:10.1016/j.heliyon.2019.e02721

Alavi, M. (1994). Tectonics of the Zagros orogenic belt of Iran: new data and interpretations. *Tectonophysics* 229, 211–238. doi:10.1016/0040-1951(94)90030-2

Aldanmaz, E. (2006). Mineral-chemical constraints on the Miocene calc-alkaline and shoshonitic volcanic rocks of Western Turkey: disequilibrium phenocryst assemblages as indicators of magma storage and mixing conditions. *Turk. J. Earth Sci.* 15, 47–73. doi:10.5194/se-11-125-2020

Ali, S. A., Buckman, S., Aswad, K. J., Jones, B. G., Ismail, S. A., and Nutman, A. P. (2013). The tectonic evolution of a Neo-Tethyan (Eocene-Oligocene) island-arc (Walash and Naopurdan groups) in the kurdistan region of the northeast Iraqi Zagros suture zone. *Isl. Arc.* 22, 104–125. doi:10.1111/iar.12007

Ali, S. A., Ismail, S. A., Nutman, A. P., Bennett, V. C., Jones, B. G., and Buckman, S. (2016). The intra-oceanic Cretaceous (~108 Ma) Kata-Rash arc fragment in the Kurdistan segment of Iraqi Zagros Suture Zone: implications for Neotethys evolution and closure. *Lithos* 260, 154–163. doi:10.1016/j.lithos.2016.05.027

Alirezaei, S., and Hassanzadeh, J. (2012). Geochemistry and zircon geochronology of the Permian a-type Hasanrobat granite, Sanandaj–Sirjan belt: a new record of the Gondwana break-up in Iran. *Lithos* 151, 122–134. doi:10.1016/j.lithos.2011.11.015

Alishah, F. P., Jahangiri, A., and Branch, S. (2013). Adakitic volcanism in Sahand region, northwest Iran: geochemical and geodynamic implications. *Phys. Sci. Res. Int.* 1, 62–75. doi:10.1155/2013/735498

Allen, M. B., Kheirkhah, M., Neill, I., Emami, M. H., and McLeod, C. L. (2013a). Generation of arc andwithin-plate chemical signatures in collision zone magmatism: quaternary lavas from kurdistan province, Iran. *J. Petrol.* 54, 887–911. doi:10.1093/petrology/egs090

Allen, M. B., Saville, C., Blanc, E. J.-P., Talebian, M., and Nissen, E. (2013b). Orogenic plateau growth: expansion of the Turkish-Iranian Plateau across the Zagros fold-and-thrust belt. *Tectonics* 32, 171–190. doi:10.1002/tect.20025

Alpaslan, M., Frei, R., Boztug, D., Kurt, M. A., and Temel, A. (2004). Geochemical and Pb-Sr-Nd isotopic constraints indicating an enriched-mantle source for late cretaceous to early tertiary volcanism, central anatolia, Turkey. *Int. Geol. Rev.* 46, 1022–1041. doi:10.2747/0020-6814.46.11.1022

An, Y., and Harrison, T. M. (2000). Geologic evolution of the Himalayan-Tibetan orogen. *Annu. Rev. Earth Planet Sci.* 28, 211–280. doi:10.1146/annurev.earth.28.1.211

Ansari, M. R., Abedini, M. V., Zadeh, A. D., Sheikhzakariaee, S. J., and Mirzaee Beni, Z. H. (2011). Geochemical constrain on the Early Cretaceous, OIB-type alkaline volcanic rocks in Kojor volcanic field, Central Alborz Mountain, north of Iran. *Aust. J. Basic Appl. Sci.* 5, 913–925.

Ansari, M. R. (2013). Geochemistry of mid cretaceous alkaline volcanic rocks, member of chaloos formation, Abbas Abad volcanic field, Central Alborz Mountains, North of Iran. *Life Sci. J.* 10, 874–883. doi:10.1155/2013/735498

Ashrafi, N., Jahangiri, A., Hasebe, N., and Eby, G. N. (2018). Petrology, geochemistry and geodynamic setting of Eocene-Oligocene alkaline intrusions from the Alborz-Azerbaijan magmatic belt, NW Iran. *Geochemistry* 78, 432–461. doi:10.1016/j.chemer.2018.10.004

Asiabanha, A., Bardintzeff, J. M., and Veysi, S. (2018). North Qorveh volcanic field, western Iran: eruption styles, petrology and geological setting. *Mineral. Petrol.* 112, 501–520. doi:10.1007/s00710-017-0541-z

Asiabanha, A., and Foden, J. (2012). Post-collisional transition from an extensional volcano-sedimentary basin to a continental arc in the Alborz Ranges, N-Iran. *Lithos* 148, 98–111. doi:10.1016/j.lithos.2012.05.014

Azizi, H., Asahara, Y., and Tsuboi, M. (2014a). Quaternary high-Nb basalts: existence of young oceanic crust under the Sanandaj–Sirjan Zone, NW Iran. *Int. Geol. Rev.* 56, 167–186. doi:10.1080/00206814.2013.821268

Azizi, H., Asahara, Y., Tsuboi, M., Takemura, K., and Razyani, S. (2014b). The role of heterogenetic mantle in the genesis of adakites northeast of Sanandaj, northwestern Iran. *Chemie der Erde - Geochemistry* 74, 87–97. doi:10.1016/j.chemer.2013.09.008

Azizi, H., Chung, S. L., Tanaka, T., and Asahara, Y. (2011). Isotopic dating of the Khoy metamorphic complex (KMC), northwestern Iran: a significant revision of the formation age and magma source. *Precambrian Res.* 185, 87–94. doi:10.1016/j.precamres.2010.12.004

Azizi, H., Hadad, S., Stern, R. J., and Asahara, Y. (2019). Age, geochemistry, and emplacement of the ~40 Ma Baneh granite–appinite complex in a transpressional tectonic regime, Zagros suture zone, northwest Iran. *Int. Geol. Rev.* 61, 195–223. doi:10.1080/00206814.2017.1422394

Azizi, H., Hadi, A., Asahara, Y., and Mohammad, Y. O. Y. (2013). Geochemistry and geodynamics of the Mawat mafic complex in the Zagros Suture zone, northeast Iraq. *Cent. Eur. J. Geosci.* 5, 523–537. doi:10.2478/s13533-012-0151-6

Azizi, H., and Jahangiri, A. (2008). Cretaceous subduction–related volcanism in the northern Sanandaj–Sirjan Zone, Iran. *J. Geodyn.* 45, 178–190. doi:10.1016/j.jog.2007.11.001

Azizi, H., Lucci, F., Stern, R. J., Hasannejad, S., and Asahara, Y. (2018a). The Late Jurassic Panjeh submarine volcano in the northern Sanandaj-Sirjan Zone, northwest Iran: mantle plume or active margin?. *Lithos* 308 (309), 364–380. doi:10.1016/j.lithos.2018.03.019

Azizi, H., Mehrabi, B., and Akbarpour, A. (2009). Genesis of tertiary magnetite-apatite deposits, Southeast of Zanjan, Iran. *Resour. Geol.* 59, 330–341. doi:10.1111/j.1751-3928.2009.00101.x

Azizi, H., and Moinevaziri, H. (2009). Review of the tectonic setting of Cretaceous to Quaternary volcanism in northwestern Iran. *J. Geodyn.* 47, 167–179. doi:10.1016/j.jog.2008.12.002

Azizi, H., Nouri, F., Stern, R. J., Azizi, M., Lucci, F., Asahara, Y., et al. (2018b). New evidence for Jurassic continental rifting in the northern Sanandaj Sirjan Zone, western Iran: the Ghalaylan seamount, southwest Ghorveh. *Int. Geol. Rev.* 68, 142. doi:10.1080/00206814.2018.1535913

Azizi, H., and Stern, R. J. (2019). Jurassic igneous rocks of the central Sanandaj–Sirjan zone (Iran) mark a propagating continental rift, not a magmatic arc. *Terra. Nova.* 31, 415–423. doi:10.1111/ter.12404

Badr, A., Davoudian, A. R., Shabanian, N., Azizi, H., Asahara, Y., Neubauer, F., et al. (2018). A- and I-type metagranites from the north shahrekord metamorphic complex, Iran: evidence for early paleozoic post-collisional magmatism. *Lithos* 300–301, 86–104. doi:10.1016/j.lithos.2017.12.008

Castro, A., Aghazadeh, M., Badrzadeh, Z., and Chichorro, M. (2013). Late Eocene–Oligocene post-collisional monzonitic intrusions from the Alborz magmatic belt, NW Iran. An example of monzonite magma generation from a metasomatized mantle source. *Lithos* 180–181, 109–127. doi:10.1016/j.lithos.2013.08.003

Chiu, H. Y., Chung, S. L., Zarrinkoub, M. H., Mohammadi, S. S., Khatib, M. M., and Iizuka, Y. (2013). Zircon U-Pb age constraints from Iran on the magmatic evolution related to Neotethyan subduction and Zagros orogeny. *Lithos* 162 (163), 70–87. doi:10.1016/j.lithos.2013.01.006

Dabiri, R., Emami, M., Mollaei, H., Chen, B., Abedini, M., Omran, N., et al. (2011). Quaternary post-collision alkaline volcanism NW of Ahar (NW Iran): geochemical constraints of fractional crystallization process. *Geol. Carpathica.* 62, 547–562. doi:10.2478/v10096-011-0039-2

Davoudian, A. R., Genser, J., Dachs, E., and Shabanian, N. (2008). Petrology of eclogites from north of shahrekord, sanandaj-sirjan zone, Iran. *Mineral. Petrol.* 92, 393–413. doi:10.1007/s00710-007-0204-6

Defant, M. J., and Drummond, M. S. (1990). Derivation of some modern arc magmas by melting of young subducted lithosphere. *Nature* 347, 662–665. doi:10.1038/347662a0

Dewey, J. F., Pitman, W. C., Ryan, W. B. F., and Bonnin, J. (1973). Plate tectonics and the evolution of the alpine system. *Geol. Soc. Am. Bull.* 84, 3137. doi:10.1130/0016-7606(1973)84<3137:PTATEO>2.0.CO;2

Dilek, Y., and Altunkaynak, Ş. (2009). Geochemical and temporal evolution of Cenozoic magmatism in Western Turkey: mantle response to collision, slab break-off, and lithospheric tearing in an orogenic belt. *Geol. Soc. Spec. Publ.* 311, 213–233. doi:10.1144/SP311.8

Dilek, Y., Imamverdiyev, N., and Altunkaynak, Ş. (2010). Geochemistry and tectonics of Cenozoic volcanism in the Lesser Caucasus (Azerbaijan) and the peri-Arabian region: collision-induced mantle dynamics and its magmatic fingerprint. *Int. Geol. Rev.* 52, 536–578. doi:10.1080/00206810903360422

Doroozi, R., Vaccaro, C., Masoudi, F., and Petrini, R. (2016). Cretaceous alkaline volcanism in south Marzanabad, northern central Alborz, Iran: geochemistry and petrogenesis. *Geosci. Front.* 7, 937–951. doi:10.1016/j.gsf.2015.11.004

Frost, B. R., Barnes, C. G., Collins, W. J., Arculus, R. J., Ellis, D. J., and Frost, C. D. (2001). A geochemical classification for granitic rocks. *J. Petrol.* 42, 2033–2048. doi:10.1093/petrology/42.11.2033

Göncüoglu, M. C. (2010). *Introduction to the geology of Turkey: geodynamic evolution of the Pre-Alpine and Alpine terrances*. NewYork, NY: Springer, 1–69.

Ghaffari, M., Rashidnejad-Omran, N., Dabiri, R., Chen, B., and Santos, J. F. (2013). Mafic–intermediate plutonic rocks of the Salmas area, northwestern Iran: their source and petrogenesis significance. *Int. Geol. Rev.* 55, 2016–2029. doi:10.1080/00206814.2013.817067

Ghalamghash, J., Schmitt, A. K., and Chaharlang, R. (2019). Age and compositional evolution of Sahand volcano in the context of post-collisional magmatism in northwestern Iran: evidence for time-transgressive magmatism away from the collisional suture. *Lithos* 344–345, 265–279. doi:10.1016/j.lithos.2019.06.031

Ghasemi, A., and Talbot, C. J. (2006). A new tectonic scenario for the Sanandaj-Sirjan Zone (Iran). *J. Asian Earth Sci.* 26, 683–693. doi:10.1016/j.jseaes.2005.01.003

Ghazi, A. M., Pessagno, E. A., Hassanipak, A. A., Kariminia, S. M., Duncan, R. A., and Babaie, H. A. (2003). Biostratigraphic zonation and 40Ar–39Ar ages for the Neotethyan Khoy ophiolite of NW Iran. *Palaeogeogr. Palaeoclimatol. Palaeoecol* 193, 311–323. doi:10.1016/S0031-0182(03)00234-7

Golonka, J. (2004). Plate tectonic evolution of the southern margin of Eurasia in the Mesozoic and Cenozoic. *Tectonophysics* 381, 235–273. doi:10.1016/j.tecto.2002.06.004

Haghighi Bardineh, S. N., Zarei Sahamieh, R., Zamanian, H., and Ahmadi Khalaji, A. (2018). Geochemical, Sr-Nd isotopic investigations and U-Pb zircon chronology of the Takht granodiorite, west Iran: evidence for post-collisional magmatism in the northern part of the Urumieh-Dokhtar magmatic assemblage. *J. Afr. Earth Sci.* 139, 354–366. doi:10.1016/j.jafrearsci.2017.12.030

Haghnazar, S., and Malakotian, S. (2009). Petrography and Geochemistry of the Javaherdasht basalts (east of Guilan Province): the investigation of the role of crystal fractionation and crustal contamination in the magmatic evolution. *Mineral. Iran. J. Crystallogr. Mineral* 88, 253–266. doi:10.1016/0040-1951(94)90030-2

Haghnazar, S., Shafeie, Z., and Sharghy, Z. 2 (2016). Petrogenesis and tectonic setting of an basalt-Trachyte-Rhyolite suite in the Spilli area (south of Siahkal), north of Iran: evidences of continental rift-related bimodal magmatism in Alborz. *Ranian J. Petrol.* 27, 43–60. doi:10.22108/ijp.2016.21017

Hajialioghli, R., Moazzen, M., Jahangiri, A., Oberhänsli, R., Mocek, B., and Altenberger, U. (2011). Petrogenesis and tectonic evolution of metaluminous sub-alkaline granitoids from the Takab complex, NW Iran. *Geol. Mag.* 148, 250–268. doi:10.1017/S0016756810000683

Hassanipak, A. A., and Ghazi, A. M. (2000). Petrology, geochemistry and tectonic setting of the Khoy ophiolite, northwest Iran: implications for Tethyan tectonics. *J. Asian Earth Sci.* 18, 109–121. doi:10.1016/S1367-9120(99)00023-1

Hassanzadeh, J., and Wernicke, B. P. (2016). The Neotethyan Sanandaj-Sirjan zone of Iran as an archetype for passive margin-arc transitions. *Tectonics.* 35, 586–621. doi:10.1002/2015TC003926

Ismail, S. A., Mirza, T. M., and Carr, P. F. (2010). Platinum-group elements geochemistry in podiform chromitites and associated peridotites of the mawat ophiolite , northeastern Iraq. *J. Asian Earth Sci.* 37, 31–41. doi:10.1016/j.jseaes.2009.07.005

Jafari Sough, R., Asiabanha, A., and Nasrabadi, M. (2018). Geochemistry of Cretaceous hydromagmatic lava flows in Separdeh district, NE Qazvin, central Alborz. *Ranian J. Crystallogr. Mineral.* 26, 717–732. http://ijcm.ir/article-1-1154-fa.html.

Jahangiri, A. (2007). Post-collisional Miocene adakitic volcanism in NW Iran: geochemical and geodynamic implications. *J. Asian Earth Sci.* 30, 433–447. doi:10.1016/j.jseaes.2006.11.008

Jassim, S. Z., and Goff, J. C. (2006). *Geology of Iraq. DOLIN, sro, distributed*. London, UK: Geological Society of London.

Karim, K. H., and Al-Bidry, M. (2020). Zagros metamorphic core complex: example from bulfat mountain, qala diza area, kurdistan region, northeast Iraq. *Jordan J. Earth Environ. Sci.* 11, 113–125

Khalatbari-Jafari, M., Juteau, T., Bellon, H., and Emami, H. (2003). Discovery of two ophiolite complexes of different ages in the Khoy area (NW Iran). *Compt. Rendus Geosci.* 335, 917–929. doi:10.1016/S1631-0713(03)00123-8

Khalatbari-Jafari, M., Juteau, T., Bellon, H., Whitechurch, H., Cotten, J., and Emami, H. (2004). New geological, geochronological and geochemical investigations on the Khoy ophiolites and related formations, NW Iran. *J. Asian Earth Sci.* 23, 507–535. doi:10.1016/j.jseaes.2003.07.005

Kheirkhah, M., Allen, M. B., and Emami, M. (2009). Quaternary syn-collision magmatism from the Iran/Turkey borderlands. *J. Volcanol. Geoth. Res.* 182, 1–12. doi:10.1016/j.jvolgeores.2009.01.026

Kheirkhah, M., Neill, I., Allen, M. B., and Ajdari, K. (2013). Small-volume melts of lithospheric mantle during continental collision: late Cenozoic lavas of Mahabad, NW Iran. *J. Asian Earth Sci.* 74, 37–49. doi:10.1016/j.jseaes.2013.06.002

Kroner, U., and Romer, R. L. (2013). Two plates - many subduction zones: the Variscan orogeny reconsidered. *Gondwana Res.* 24, 298–329. doi:10.1016/j.gr.2013.03.001

Le Bas, M., Maitre, R., Streckeisen, A., and Zanettin, B. (1986). A chemical classification of volcanic rocks based on the total alkali-silica diagram. *J. Petrol.* 27, 745–750. doi:10.1093/petrology/27.3.745

Lechmann, A., Burg, J.-P. P., Ulmer, P., Mohammadi, A., Guillong, M., and Faridi, M. (2018). From Jurassic rifting to Cretaceous subduction in NW Iranian Azerbaijan: geochronological and geochemical signals from granitoids. *Contrib. Mineral. Petrol.* 173, 102. doi:10.1007/s00410-018-1532-8

Mahmoudi, S., Corfu, F., Masoudi, F., Mehrabi, B., and Mohajjel, M. (2011). U-Pb dating and emplacement history of granitoid plutons in the northern Sanandaj-Sirjan Zone, Iran. *J. Asian Earth Sci.* 41, 238–249. doi:10.1016/j.jseaes.2011.03.006

Manafi, M., Arian, M., Raeesi, S. H. T., and Solgi, A. (2013). Tethys subduction history in Caucasus region. *Open J. Geol.* 03, 222–232. doi:10.4236/ojg.2013.33026

Mazhari, S. A., Amini, S., Ghalamghash, J., and Bea, F. (2011). Petrogenesis of granitic unit of naqadeh complex, Sanandaj–Sirjan zone, NW Iran. *Arab. J. Geosci.* 4, 59–67. doi:10.1007/s12517-009-0077-6

Mazhari, S. A., Bea, F., Amini, S., Ghalamghash, J., Molina, J. F., Montero, P., et al. (2009). The Eocene bimodal Piranshahr massif of the Sanandaj-Sirjan Zone, NW Iran: a marker of the end of the collision in the Zagros orogen. *J. Geol. Soc. London* 166, 53–69. doi:10.1144/0016-76492008-022

Mehrabi, B., Siani, M. G. M. G., Goldfarb, R., Azizi, H., Ganerod, M., and Marsh, E. E. (2016). Mineral assemblages, fluid evolution, and genesis of polymetallic epithermal veins, Glojeh district, NW Iran. *Ore Geol. Rev.* 78, 41–57. doi:10.1016/j.oregeorev.2016.03.016

Miyazaki, T., Hanyu, T., Kimura, J.-I., Senda, R., Vaglarov, B. S., Chang, Q., et al. (2018). Clinopyroxene and bulk rock Sr–Nd–Hf–Pb isotope compositions of Raivavae ocean island basalts: does clinopyroxene record early stage magma chamber processes?. *Chem. Geol.* 482, 18–31. doi:10.1016/j.chemgeo.2017.12.015

Moghadam, H. S., Ghorbani, G., Khedr, M. Z., Fazlnia, N., Chiaradia, M., Eyuboglu, Y., et al. (2014). Late Miocene K-rich volcanism in the eslamieh peninsula (saray), NW Iran: implications for geodynamic evolution of the Turkish–Iranian high plateau. *Gondwana Res.* 26, 1028–1050. doi:10.1016/j.gr.2013.09.015

Moghadam, H. S., and Stern, R. J. (2015). Ophiolites of Iran: keys to understanding the tectonic evolution of SW Asia: (II) Mesozoic ophiolites. *J. Asian Earth Sci.* 100, 31–59. doi:10.1016/j.jseaes.2014.12.016

Mohammad, Y. O., and Cornell, D. H. (2017). U–Pb zircon geochronology of the Daraban leucogranite, Mawat ophiolite, Northeastern Iraq: a record of the subduction to collision history for the Arabia–Eurasia plates. *Isl. Arc.* 26, e12188. doi:10.1111/iar.12188

Mohammad, Y. O. (2013). P–T evolution of meta-peridotite in the Penjwin ophiolite, northeastern Iraq. *Arab. J. Geosci.* 6, 505–518. doi:10.1007/s12517-011-0372-x

Moritz, R., Rezeau, H., Ovtcharova, M., Tayan, R., Melkonyan, R., Hovakimyan, S., et al. (2016). Long-lived, stationary magmatism and pulsed porphyry systems during Tethyan subduction to post-collision evolution in the southernmost Lesser Caucasus, Armenia and Nakhitchevan. *Gondwana Res.* 37, 465–503. doi:10.1016/j.gr.2015.10.009

Neill, I., Meliksetian, K., Allen, M. B., Navasardyan, G., and Kuiper, K. (2015). Petrogenesis of mafic collision zone magmatism: the Armenian sector of the Turkish-Iranian Plateau. *Chem. Geol.* 403. doi:10.1016/j.chemgeo.2015.03.013

Nouri, F., Asahara, Y., Azizi, H., and Tsuboi, M. (2019). Petrogenesis of the Harsin–Sahneh serpentinized peridotites along the Zagros suture zone, western Iran: new evidence for mantle metasomatism due to oceanic slab flux. *Geol. Mag.* 156, 772–800. doi:10.1017/S0016756818000201

Nouri, F., Asahara, Y., Azizi, H., Yamamoto, K., and Tsuboi, M. (2017). Geochemistry and petrogensis of the Eocene back arc mafic rocks in the Zagros suture zone, northern Noorabad, western Iran. *Chemie der Erde Geochem.* 77, 517–533. doi:10.1016/j.chemer.2017.06.002

Nouri, F., Azizi, H., Asahara, Y., and Stern, R. J. (2020). A new perspective on Cenozoic calc-alkaline and shoshonitic volcanic rocks, eastern Saveh (central Iran). *Int. Geol. Rev.* 17, 185. doi:10.1080/00206814.2020.1718005

Nouri, F., Azizi, H., Golonka, J., Asahara, Y., Orihashi, Y., Yamamoto, K., et al. (2016). Age and petrogenesis of Na-rich felsic rocks in western Iran: evidence for closure of the southern branch of the Neo-Tethys in the Late Cretaceous. *Tectonophysics* 671, 151–172. doi:10.1016/j.tecto.2015.12.014

Parlak, O., HÖck, V., and Delaloye, M. (2000). Suprasubduction zone origin of the pozanti-karsanti ophiolite (southern Turkey) deduced from whole-rock and mineral chemistry of the gabbroic cumulates. *Geol. Soc. London, Spec. Publ.* 173, 219–234. doi:10.1144/GSL.SP.2000.173.01.11

Pearce, J. A. (2008). Geochemical fingerprinting of oceanic basalts with applications to ophiolite classification and the search for Archean oceanic crust. *Lithos* 100, 14–48. doi:10.1016/j.lithos.2007.06.016

Pearce, J. A., Harrison, N. B. W., and Tindel, A. G. (1984). Trace element discrimination diagrams for the tectonic Iinterpretation of granitic rocks. *J. Petrol.* 25, 956–983. doi:10.1093/petrology/25.4.956

Pearce, J. A. (1982). "*Trace element characteristics of lavas from destructive plate boundaries*", in *In andesites: orogenic andesites and related rocks.* (New York, NY: Wiley), 525–548

Prelević, D., and Seghedi, I. (2013). Magmatic response to the post-accretionary orogenesis within Alpine-Himalayan belt-Preface. *Lithos* 180–181, 1–4. doi:10.1016/j.lithos.2013.09.004

Rabiee, A., Rossetti, F., Tecce, F., Asahara, Y., Azizi, H., Glodny, J., et al. (2019). Multiphase magma intrusion, ore-enhancement and hydrothermal carbonatisation in the Siah-Kamar porphyry Mo deposit, Urumieh-Dokhtar magmatic zone, NW Iran. *Ore Geol. Rev.* 110, 102930. doi:10.1016/j.oregeorev.2019.05.016

Ranin, A., Sepahi, A. A., Moein-Vaziri, H., and Aliani, F. (2010). Petrology and geochemistry of the plutonic complexes of the Marivan area, Sanandaj-Sirjan zone (In Farsi with English abstract). *Petrology*, 22, 43–60.

Sahakyan, L., Bosch, D., Sosson, M., Avagyan, A., Galoyan, G., Rolland, Y., et al. (2017). Geochemistry of the Eocene magmatic rocks from the Lesser Caucasus area (Armenia): evidence of a subduction geodynamic environment. *Geol. Soc. London, Spec. Publ.* 428, 73–98. doi:10.1144/SP428.12

Sclater, J. G., Anderson, R. N., and Bell, M. L. (1971). Elevation of ridges and evolution of the central eastern Pacific. *J. Geophys. Res.* 76, 7888–7915. doi:10.1029/jb076i032p07888

Shabanian, N., Davoudian, A. R., Dong, Y., and Liu, X. (2018). U-Pb zircon dating, geochemistry and Sr-Nd-Pb isotopic ratios from Azna-Dorud Cadomian metagranites, Sanandaj-Sirjan Zone of western Iran. *Precambrian Res.* 306, 41–60. doi:10.1016/j.precamres.2017.12.037

Shafaii Moghadam, H., Corfu, F., Stern, R. J., and Lotfi Bakhsh, A. (2019). The eastern Khoy metamorphic complex of NW Iran: a jurassic ophiolite or continuation of the sanandaj–sirjan zone. *J. Geol. Soc. London* 177, 517–529. doi:10.1144/jgs2018-081

Shafaii Moghadam, H., Griffin, W. L., Kirchenbaur, M., Garbe-Schönberg, D., Zakie Khedr, M., Kimura, J.-I., et al. (2018). Roll-back, extension and mantle upwelling triggered Eocene potassic magmatism in NW Iran. *J. Petrol.* 59, 1417–1465. doi:10.1093/petrology/egy067

Shafaii Moghadam, H., and Stern, R. J. (2014). Ophiolites of Iran: keys to understanding the tectonic evolution of SW Asia: (I) Paleozoic ophiolites. *J. Asian Earth Sci.* 91, 19–38. doi:10.1016/j.jseaes.2014.04.008

Shervais, J. W. (1982). Ti-V plots and the petrogenesis of modern and ophiolitic lavas. *Earth Planet Sci. Lett.* 59, 101–118. doi:10.1016/0012-821X(82)90120-0

Siani, M. G., Mehrabi, B., Azizi, H., Wilkinson, C. M., and Ganerod, M. (2015). Geochemistry and geochronology of the volcano-plutonic rocks associated with the Glojeh epithermal gold mineralization, NW Iran. *Open Geosci.* 7. doi:10.1515/geo-2015-0024

Stöcklin, J., and Nabavi, M. H. (1973). *Tectonic map of Iran, scale 1:2,500,000.* Tehran: Geological Survey of Iran.

Sun, S. S., and McDonough, W. F. (1989). Chemical and isotopic systematics of oceanic basalts: implications for mantle composition and processes. *Geol. Soc. London, Spec. Publ.* 42, 313–345. doi:10.1144/GSL.SP.1989.042.01.19

Taki, S. (2017). The role of fractional crystallization in the evolution of magma of the Upper Cretaceous volcanic and subvolcanic rocks from the Nageleh Sar Syncline, south Mahmood Abad, North Iran. *Iran. J. Crystallogr. Mineral.* 25, 50–522. doi:10.1029/2010TC002809

Temizel, İ., Arslan, M., Yücel, C., Yazar, E. A., Kaygusuz, A., and Aslan, Z. (2019). U-Pb geochronology, bulk-rock geochemistry and petrology of Late Cretaceous syenitic plutons in the Gölköy (Ordu) area (NE Turkey): implications for magma generation in a continental arc extension triggered by slab roll-back. *J. Asian Earth Sci.* 171, 305–320. doi:10.1016/j.jseaes.2019.01.004

Tian, S. H., Yang, Z. Sen., Hou, Z. Q., Mo, X. X., Hu, W. J., Zhao, Y., et al. (2017). Subduction of the Indian lower crust beneath southern Tibet revealed by the post-collisional potassic and ultrapotassic rocks in SW Tibet. *Gondwana Res.* 41, 29–50. doi:10.1016/j.gr.2015.09.005

Topuz, G., Altherr, R., Satir, M., and Schwarz, W. H. (2004). Low-grade metamorphic rocks from the Pulur complex, NE Turkey: implications for the pre-Liassic evolution of the Eastern Pontides. *Int. J. Earth Sci.* 93, 72–91. doi:10.1007/s00531-003-0372-5

Topuz, G., Candan, O., Zack, T., and Yılmaz, A. (2017). East Anatolian plateau constructed over a continental basement: no evidence for the East Anatolian accretionary complex. *Geology.* 45, 791–794. doi:10.1130/G39111.1

Torkian, A., Furman, T., Salehi, N., and Veloski, K. (2019). Petrogenesis of adakites from the Sheyda volcano, NW Iran. *J. Afr. Earth Sci.* 150, 194–204. doi:10.1016/j.jafrearsci.2018.11.014

Torkian, A., Salehi, N., and Siebel, W. (2016). Geochemistry and petrology of basaltic lavas from NE-Qorveh, Kurdistan province, Western Iran. *Abhandlungen J. Mineral. Geochem.* 193, 95–128. doi:10.1127/njma/2016/0296

Whitechurch, H., Omrani, J., Agard, P., Humbert, F., Montigny, R., and Jolivet, L. (2013). Evidence for Paleocene-Eocene evolution of the foot of the Eurasian margin (Kermanshah ophiolite, SW Iran) from back-arc to arc: implications for regional geodynamics and obduction. *Lithos.* 182 (183), 11–32. doi:10.1016/j.lithos.2013.07.017

Wrobel-Daveau, J. C., Ringenbach, J. C., Tavakoli, S., Ruiz, G. M. H., Masse, P., and Frizon de Lamotte, D. (2010). Evidence for mantle exhumation along the Arabian margin in the Zagros (Kermanshah area, Iran). *Arab. J. Geosci.* 3, 499–513. doi:10.1007/s12517-010-0209-z

Zaeimnia, F., Arai, S., and Mirmohammadi, M. (2017). Na-rich character of metasomatic/metamorphic fluids inferred from preiswerkite in chromitite pods of the Khoy ophiolite in Iran: role of chromitites as capsules of trapped fluids. *Lithos.* 268–271, 351–363. doi:10.1016/j.lithos.2016.11.021

Zhang, Z., Dong, D., Sun, W., Zhang, G., and Bai, Y. (2020). Investigation of an oceanic plateau formation and rifting initiation model implied by the Caroline Ridge on the Caroline Plate, western Pacific. *Int. Geol. Rev.* 71, 100. doi:10.1080/00206814.2019.1707126

Zhang, Z., Ji, W., Majidifard, M. R., Rezaeian, M., Talebian, M., Xiang, D., et al. (2018). Geochemistry, zircon U-Pb and Hf isotope for granitoids, NW Sanandaj-Sirjan zone, Iran: implications for Mesozoic-Cenozoic episodic magmatism during Neo-Tethyan lithospheric subduction. *Gondwana Res.* 62, 227–245. doi:10.1016/j.gr.2018.04.002

Conflict of Interest: The authors declare that the research was conducted in the absence of any commercial or financial relationships that could be construed as a potential conflict of interest.